Applied Surface Science Advances 18 (2023) 100472

Contents lists available at ScienceDirect

Applied Surface Science Advances

journal homepage: www.sciencedirect.com/journal/applied-surface-science-advances

Critical overview and comparison between models for adsorption-desorption noise in bio-chemical sensors

Fabrizio Bettetti [a], Leandro Julian Mele [b], Pierpaolo Palestri [*,a]

[a] DPIA, University of Udine, Via delle Scienze 206, Udine, 33100, UD, Italy
[b] Department of Materials Science and Engineering, Stanford University, Stanford, 94305, CA, USA

ARTICLE INFO

Keywords:
Adsorption-desorption noise
Bio-chemical sensors
Kinetic Monte Carlo

ABSTRACT

We critically review existing models for the adsorption-desorption noise in bio-chemical sensors, in particular the model based on simplified forward Kolmogorov equation and the models based on Langevin sources. For the latter models, we propose a generalized version to handle cases beyond the branched surface reactions (a binding site that can be alternatively occupied by different ions/molecules) and the chained reaction (a binding site that sequentially binds with ions/molecules). The models are benchmarked against kinetic Monte Carlo (kMC) simulations considering relevant case studies such as pH-sensitive ions, selective molecules binding on a functionalized surface and multi-layer adsorption on bare surfaces. It is found that although the mathematical formulation of the modeling approaches appears different, when dealing with independent binding sites, they are fully equivalent and perfectly match the kMC results. The case of competitive binding considering the correlation between the occupation of the binding sites has also been analyzed.

1. Introduction

Biosensors are devices able to interact with target analytes and to convert such interaction into a viable physical quantity, typically a voltage difference, an electric current, or changes in a resonance frequency [1]. The major challenge of these sensors is that the target analyte is always present in a multianalyte environment, where one or more (interfering) species can interact similarly with the sensing element, thus limiting selectivity. In conventional ion-sensitive field effect transistors (ISFETs), the target analytes are ions involved in a sequence of binding events that determine the surface charge density at the gate channel [2,3]. But regardless of whether the analyte is involved in a chained cascade of binding events, competing with interfering species, or even a combination of the two cases, the knowledge of such surface mechanisms is fundamental for the interpretation of the sensor response. For pH-sensitive ISFETs, chained reaction events are described by the so-called site-binding (SB) model [4].

If the number of sensing sites is small, i.e., when sensing small concentrations of the analyte or even in single-molecule detection, the kinetics of the binding events resulting from binding/unbinding fluctuations (see top panel in Fig. 1) convey additional information that is also transduced by the sensor. The spectral information encoded in such signals (lower right panel in Fig. 1) can be used to distinctively uncouple processes according to their characteristic frequencies [5–7]. To this aim, modeling frameworks addressing the chemical noise (i.e., compute the power-spectral density, PSD, of the fluctuations) for specific reactions have been proposed in the literature [6,8,9]. Recently, two independent works [10,11] have also addressed this problem from a wider perspective, providing a general framework to calculate the spectral noise of adsorption/desorption processes based on an arbitrary set of surface reactions.

In this work, we critically compare the modeling approaches for adsorption/desorption noise considering some relevant case studies ranging from pH sensing to molecule deposition on sensing surfaces. Furthermore, these models are compared with kinetic Monte Carlo (kMC) simulations. We also propose a methodology to extend the approach of [11,12] to arbitrarily complex surface reactions, although limited to independent binding sites.

The manuscript proceeds as follows. After introducing the general framework and the use of the Markov chains to describe the evolution during time of the state of independent surface sites, Section 2 describes the different models (the one based on the simplified forward Kolmogorov equation and the ones based on Langevin sources) as well as the kMC simulator. Simulation results for independent surface sites are

* Corresponding author.
E-mail address: pierpaolo.palestri@uniud.it (P. Palestri).

https://doi.org/10.1016/j.apsadv.2023.100472
Received 1 August 2023; Received in revised form 3 October 2023; Accepted 10 October 2023
Available online 25 October 2023

provided in Section 3. The effect of the correlation between sites in the case of competitive binding on a sensing surface is discussed in Section 4. Conclusions are drawn in Section 5.

2. Description of the modeling approaches for independent binding sites

2.1. General framework

We consider a surface with N_{sites} binding sites with the same properties. The sites are independent, so one can derive the statistical properties of a single site and then extend the analysis to multiple sites. In particular, we will deal with the power-spectral-density (PSD) of the fluctuations around a steady-state condition. The overall PSD is thus the PSD of the fluctuations associated to a single site multiplied by N_{sites}.

The adsorption-desorption of analytes on the binding sites can be described by a Markov chain where the site evolves toward different *states* during the time following a Poisson process. For example, in the simplest situation, a site can be in the states *empty* or *occupied*. In the steady state, a fraction of sites will be empty and a fraction will be occupied. In any case, a single site will oscillate between the two states, giving rise to *adsorption-desorption noise*. In general, the states can be more than two. For example in the site-binding model for adsorption of protons on oxide surfaces, the site can capture one or two protons or be deprotonated, so it can be in three different states.

A powerful way to describe a general situation is by using graphs to represent the Markov chain [10,13]. Two relevant examples are reported in Fig. 2: a *branched process* (left plot), representative of selective and exclusive binding of different analytes on the site (e.g. the site can capture analyte A or analyte B, etc.), and a *chained process* where different analytes can be captured sequentially by the same site (e.g., a site on an oxide surface capturing one proton and then a second one or the same site over which many layers of analyte can accumulate). These will be analyzed as relevant cases in the following, although the theory presented here is general and can be applied to graphs with arbitrary topology.

To describe the time evolution of a site, we employ the *Kolmogorov's forward equations*:

$$\frac{d\boldsymbol{P}(t)}{dt} = \boldsymbol{G}\boldsymbol{P}(t), \tag{1}$$

where $\boldsymbol{P}(t)$ is the vector of elements P_j representing the probability for a binding site to be in state j. Note that if we have N states numbered from 0 to $N-1$, it holds that:

$$\sum_{j=0}^{N-1} P_j(t) = 1. \tag{2}$$

The matrix $\boldsymbol{G}$ contains the transition probability per unit time: G_{ij} is the probability per unit time for a site to jump from state j to state i, as indicated in the arrow connecting the different states in Fig. 2. In principle, the elements of $\boldsymbol{G}$ may depend on $\boldsymbol{P}(t)$, see for example the situation of competitive binding of molecules on a surface discussed in [12]. This induces a sort of correlation between the occupation of the different sites. In this paper, we consider models that assume the sites to be uncorrelated. An example of correlation between sites will be discussed in Section 4.

The output of the sensor corresponding to the state of a single binding site is given by

$$x_{out} = \sum_{j=0}^{N-1} x_j P_j = \boldsymbol{x}^T \boldsymbol{P} \tag{3}$$

where $\boldsymbol{x}$ is the vector containing the values of the physical variable related to the state of the binding site. For example, if the sensor response is related to the surface charge concentration (as in [10,13]) we can write $x_j = qz_j/A$, where q is the elementary charge, z_j the valence of the site in state j and A the area of the sensing element. If instead, the relevant physical variable is the mass of the analyte(s) sticking in the site, x_j will be the mass of the analytes present on the site when in state j.

At equilibrium, we have:

$$\boldsymbol{G}\boldsymbol{P}^0 = \boldsymbol{0} \tag{4}$$

where $\boldsymbol{P}^0$ is the vector containing the probability of being in a certain state at equilibrium. It is easy to show that if the Markov chain describing the transitions between states does not contain loops, we have that

$$G_{ij}P_j^0 = G_{ji}P_i^0. \tag{5}$$

This property has been exploited in [13] to derive a procedure to obtain the vector $\boldsymbol{P}^0$ for an arbitrary set of surface reactions in potentiometric sensors.

When dealing with adsorption-desorption noise, we are looking to deviations $\Delta P_i(t)$ with respect to P_i^0. Since Eq. (2) holds we need to find a vector $\boldsymbol{\Delta P}$ with size $N-1$. In this case Eq. (1) becomes:

$$\frac{d\boldsymbol{\Delta P}(t)}{dt} = \boldsymbol{\Omega}\boldsymbol{\Delta P}(t). \tag{6}$$

The matrix $\boldsymbol{\Omega}$ is obtained from the matrix $\mathbf{G}$ by removing one state. This

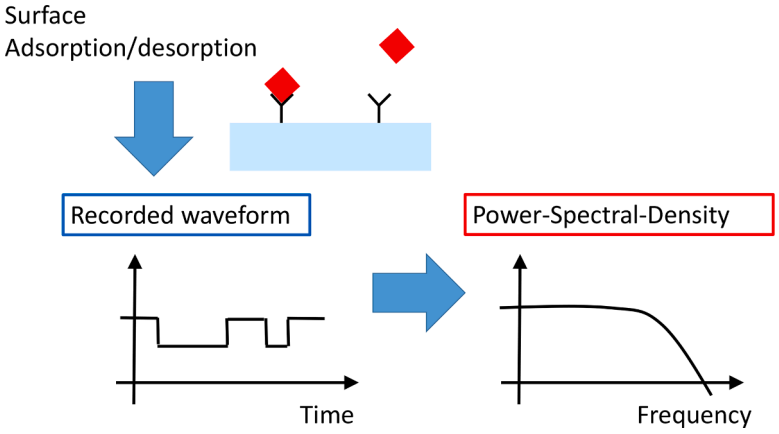

Fig. 1. Sketch of stochastic adsorption/desorption of analytes on a sensing surface. The process results in noisy sensor waveforms. The target of this paper is to compare models for the power-spectral-density of the sensor signal.

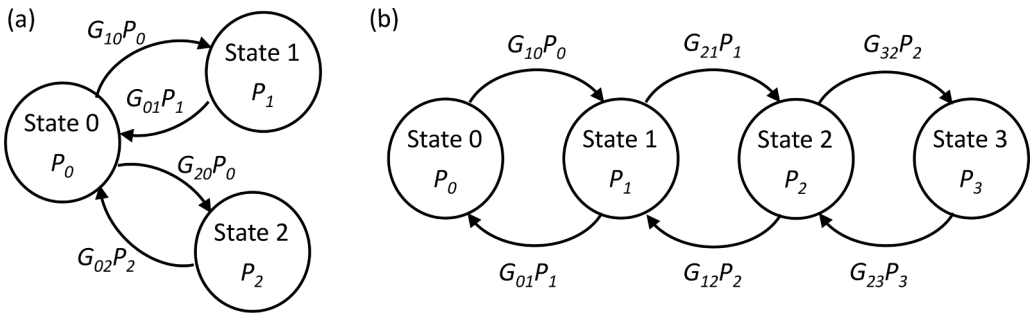

Fig. 2. Example of graphs describing the time evolution of the Markov chain representing the different possible states for a binding site. (a) Branching process. (b) Chained process. The circles represent the states, with occupation P_j, while the arrows are the transition rates (probability per unit time to jump between two states).

is done using the matrices $\boldsymbol{T}$ and $\boldsymbol{R}$ [10]:

$$\boldsymbol{\Omega} = \boldsymbol{TGR}. \tag{7}$$

For example, if state $N-1$ is removed, we have

$$\begin{aligned} &\mathbf{T} \triangleq (\boldsymbol{I} \quad \boldsymbol{0}); \\ &\boldsymbol{R} \triangleq \begin{pmatrix} \boldsymbol{I} \\ -\boldsymbol{I}^T \end{pmatrix} \end{aligned} \tag{8}$$

where $\boldsymbol{I}$ is the identity matrix of size $(N-1)\times(N-1)$, $\boldsymbol{0}$ a column vector containing $(N-1)$ elements with value 0 and $-\boldsymbol{I}^T$ is a row vector containing $(N-1)$ elements with value -1.

2.2. Model based on the forward Kolmogorov equation

The power-spectral density (PSD) vs frequency f of the fluctuations of $\boldsymbol{x}_{out}(t)$ associated to the $\boldsymbol{\Delta P}(t)$ in Eq. (6) has been derived in [10] as:

$$S_{x_{out}x_{out}}(f) = 4N_{sites}\boldsymbol{x}^T\boldsymbol{R}\boldsymbol{\Gamma}\left(\Re\left\{(j2\pi f\boldsymbol{I}-\boldsymbol{\Omega})^{-1}\right\}\right)^T\boldsymbol{R}^T\boldsymbol{x} \tag{9}$$

where the matrix $\boldsymbol{\Gamma}$ is linked to the equilibrium state probabilities:

$$\boldsymbol{\Gamma} = \begin{bmatrix} P_0^0 & \cdots & 0 \\ \vdots & \ddots & \vdots \\ 0 & \cdots & P_{N-2}^0 \end{bmatrix} - \boldsymbol{P}'^0\left(\boldsymbol{P}'^0\right)^T. \tag{10}$$

More specifically, the vector $\boldsymbol{P}'^0$ corresponds to the vector $\boldsymbol{P}^0$ after the elimination of the element corresponding to the state removed when converting $\boldsymbol{G}$ into $\boldsymbol{\Omega}$.

Notice that $\boldsymbol{P}^0$ can be computed from Eq. (4) (i.e. as the kernel of $\boldsymbol{G}$) or using the methodology described in [13].

Eq. (9) has been used in [10] to derive the *chemical noise* associated with binding-unbinding of ions in potentiometric chemical sensors. The treatment is however general and the equation can be applied to any generic situation where analytes bind to a surface.

2.3. Models using Langevin sources

Many models for adsorption-desorption noise in bio-chemical sensors based on Langevin sources have been proposed [11,12,14–16]. The equations in the above references can be re-cast using our symbols as:

$$S_{x_{out}x_{out}}(f) = N_{sites}\boldsymbol{x}^T\boldsymbol{R}(-\boldsymbol{\Omega}+j2\pi f\boldsymbol{I})^{-1}\boldsymbol{S}_\xi\left[(-\boldsymbol{\Omega}-j2\pi f\boldsymbol{I})^{-1}\right]^T\boldsymbol{R}^T\boldsymbol{x}. \tag{11}$$

The matrix $\mathbf{S}_\xi$ depends on the type of process. For branched processes (left plot of Fig. 2), it is a diagonal matrix [12]:

$$\mathbf{S}_\xi = 4\begin{bmatrix} G_{0,1}P_1^0 & \cdots & 0 \\ \vdots & \ddots & \vdots \\ 0 & \cdots & G_{0,N-1}P_{N-1}^0 \end{bmatrix} \tag{12}$$

where the state '0' is the root of the graph describing the branched relation and it is removed when converting $\mathbf{G}$ into $\boldsymbol{\Omega}$.

For chained reactions, [11] assumes that $\mathbf{S}_\xi$ is diagonal:

$$\mathbf{S}_\xi = 4\begin{bmatrix} G_{0,1}P_1^0 + G_{1,2}P_2^0 & \cdots & 0 \\ \vdots & \ddots & \vdots \\ 0 & \cdots & G_{N-2,N-1}P_{N-1}^0 \end{bmatrix} \tag{13}$$

where the state '0' is the leftmost state of the graph describing the chained relation and it is removed when constructing $\boldsymbol{\Omega}$.

One should note that Eq. (11) is actually the projection on the output vector $\mathbf{x}$ of the PSDs given by Eq. (82) [17]. So, the two cases above (Eqs. (12) and (13)) should be particular cases of the most general [17]:

$$\mathbf{S}_\xi = -2\left(\boldsymbol{\Omega\Gamma}+\boldsymbol{\Gamma\Omega}^T\right) = -4\boldsymbol{\Omega\Gamma} \tag{14}$$

where it is easy to show that the last equality comes from Eq. (5).

With some tedious matrix manipulations, one can show that Eq. (12) is indeed equivalent to Eq. (14), while this does not apply to Eq. (13). In fact the matrix $\mathbf{S}_\xi$ for chained reactions should posses also off-diagonal terms and read:

$$\mathbf{S}_\xi = 4\begin{bmatrix} G_{0,1}P_1^0 + G_{1,2}P_2^0 & -G_{1,2}P_2^0 & 0 & \cdots & 0 \\ -G_{2,1}P_1^0 & G_{1,2}P_1^1 + G_{2,3}P_3^0 & -G_{2,3}P_3^0 & \cdots & 0 \\ \vdots & \vdots & \ddots & \ddots & \vdots \\ 0 & \cdots & 0 & -G_{N-1,N-2}P_{N-2}^0 & G_{N-2,N-1}P_{N-1}^0 \end{bmatrix}. \tag{15}$$

2.4. Equivalence between the two models

Although Eqs. (9) and (11) may look quite different, we show below that, after substituting Eq. (14) into the latter, one gets exactly the same expression. In other words, it is true that:

$$\begin{aligned}&\boldsymbol{\Gamma}\left(\Re\left\{(j2\pi f\mathbf{I}-\boldsymbol{\Omega})^{-1}\right\}\right)^{T}\\&=\frac{1}{2}(-\boldsymbol{\Omega}+j2\pi f\mathbf{I})^{-1}\left(-\boldsymbol{\Omega}\boldsymbol{\Gamma}-\boldsymbol{\Gamma}\boldsymbol{\Omega}^{T}\right)\left[(-\boldsymbol{\Omega}-j2\pi f\boldsymbol{I})^{-1}\right]^{T}.\end{aligned}\tag{16}$$

The equivalence above can be proven in the following way. From the relation:

$$\boldsymbol{\Omega}\boldsymbol{\Gamma}=\boldsymbol{\Gamma}\boldsymbol{\Omega}^{T}\tag{17}$$

it follows that

$$(-\boldsymbol{\Omega}+j2\pi f\boldsymbol{I})\boldsymbol{\Gamma}=\boldsymbol{\Gamma}\left(-\boldsymbol{\Omega}^{T}+j2\pi f\boldsymbol{I}\right).\tag{18}$$

Multiplying with inverse matrix of $-\boldsymbol{\Omega}^{T}+j2\pi f\mathbf{I}$ both members, we have

$$(-\boldsymbol{\Omega}+j2\pi f\mathbf{I})\boldsymbol{\Gamma}\left(-\boldsymbol{\Omega}^{T}+j2\pi f\mathbf{I}\right)^{-1}=\boldsymbol{\Gamma}.\tag{19}$$

Multiplying both members by $\boldsymbol{\Omega}^{T}+j2\pi f\mathbf{I}$, the previous expression becomes

$$(-\boldsymbol{\Omega}+j2\pi f\mathbf{I})\boldsymbol{\Gamma}\left(-\boldsymbol{\Omega}^{T}+j2\pi f\mathbf{I}\right)^{-1}\left(\boldsymbol{\Omega}^{T}+j2\pi f\mathbf{I}\right)=\boldsymbol{\Gamma}\left(\boldsymbol{\Omega}^{T}+j2\pi f\mathbf{I}\right).\tag{20}$$

Expanding the matrix multiplication at the right-hand side, and adding $\boldsymbol{\Omega}\boldsymbol{\Gamma}$ at both members:

$$\begin{aligned}&(-\boldsymbol{\Omega}+j2\pi f\mathbf{I})\boldsymbol{\Gamma}\left(-\boldsymbol{\Omega}^{T}+j2\pi f\mathbf{I}\right)^{-1}\left(\boldsymbol{\Omega}^{T}+j2\pi f\mathbf{I}\right)+\boldsymbol{\Omega}\boldsymbol{\Gamma}-j2\pi f\boldsymbol{\Gamma}\\&=\boldsymbol{\Gamma}\boldsymbol{\Omega}^{T}+\boldsymbol{\Omega}\boldsymbol{\Gamma}.\end{aligned}\tag{21}$$

Factoring out the matrix $\boldsymbol{\Gamma}$ at the left-hand side and multiplying both members by the inverse matrix $(\boldsymbol{\Omega}^{T}+j2\pi f\mathbf{I})^{-1}$, the previous equality turns into

$$\begin{aligned}&(-\boldsymbol{\Omega}+j2\pi f\mathbf{I})\boldsymbol{\Gamma}\left(-\boldsymbol{\Omega}^{T}+j2\pi f\mathbf{I}\right)^{-1}-(-\boldsymbol{\Omega}+j2\pi f\mathbf{I})\boldsymbol{\Gamma}\left(\boldsymbol{\Omega}^{T}+j2\pi f\mathbf{I}\right)^{-1}\\&=\left(\boldsymbol{\Gamma}\boldsymbol{\Omega}^{T}+\boldsymbol{\Omega}\boldsymbol{\Gamma}\right)\left(\boldsymbol{\Omega}^{T}+j2\pi f\mathbf{I}\right)^{-1}.\end{aligned}\tag{22}$$

We can then factor out $(-\boldsymbol{\Omega}+j2\pi\mathbf{I})\boldsymbol{\Gamma}$ at the left-hand side and then multiply both members by the inverse of $(-\boldsymbol{\Omega}+j2\pi\mathbf{I})$. We get:

$$\begin{aligned}&\boldsymbol{\Gamma}\left[\left(-\boldsymbol{\Omega}^{T}+j2\pi f\mathbf{I}\right)^{-1}-\left(\boldsymbol{\Omega}^{T}+j2\pi f\mathbf{I}\right)^{-1}\right]=\\&(-\boldsymbol{\Omega}+j2\pi f\mathbf{I})^{-1}\left(\boldsymbol{\Gamma}\boldsymbol{\Omega}^{T}+\boldsymbol{\Omega}\boldsymbol{\Gamma}\right)\left(\boldsymbol{\Omega}^{T}+j2\pi f\mathbf{I}\right)^{-1}\end{aligned}\tag{23}$$

Multiplying both sides by $-1/2$ and considering that the real part of a matrix $\boldsymbol{A}$ can be written as $Re\{\boldsymbol{A}\}=\frac{1}{2}(\boldsymbol{A}+\boldsymbol{A}^{*})$ (where the * stand for the complex conjugate), one gets Eq. (16).

Since Eqs. (9) and (11) (after substituting Eq. (14)) are fully equivalent, in the following we will plot one single curve for the two models and refer to it as *general model* as opposed to the use of Eq. (11) with either Eqs. (12) or (13) that are derived for particular cases. As anticipated before it can be shown that Eqs. (11) with (12) is exact in the case of branched graphs, whereas for chained cases, Eq. (13) should be replaced by Eq. (15).

2.5. Kinetic Monte Carlo

To verify the validity of Eqs. (9) and (11) we have developed a simple kinetic Monte Carlo (kMC) algorithm to study the stochastic evolution of a single site [18].

Assuming to start with the site in state i, the site remains in this state for a time

$$\Delta t_i=-\frac{1}{\sum_{j=1,j\neq i}^{N}G_{ji}}\ln r_1\tag{24}$$

where r_1 is a random number uniformly distributed between 0 and 1.

After that time, state k is selected if

$$\sum_{j=1,j\neq i}^{k-1}G_{ji}<r_2\leq\sum_{j=1,j\neq i}^{k}G_{ji}\tag{25}$$

where also r_2 is a random number uniformly distributed between 0 and 1.

The kMC thus provides a sequence piecewise constant waveform where $x_{out}(t)=x_i$ for a time Δt_i. The Fourier transform of each of these constant steps (after subtracting the average value of $x_{out}(t)$ over the simulation time) is a *sinc* function. The combination of all these *sinc* functions gives the PSD of the random variable $x_{out}(t)$. This should be multiplied by N_{sites} to get the PSD of the whole surface.

Note that we compute the PSD considering only the second half of the time evolution of $x_{out}(t)$ to avoid any spurious effect due to the arbitrary choice of the initial state. The PSD is not plotted for frequencies below twice the inverse of the simulation time since fluctuations below that frequency are not sampled by the kMC procedure.

We have also developed a kMC for multiple independent sites and obtained exactly the same PSD as using a single site and multiplied the PSD by N_{sites}. The algorithm is more complicated and much less numerically efficient, so it is not detailed here and, in the following, we will employ the kMC for a single site.

3. Results for independent binding sites

The equivalence between the PSD provided by Eqs. (9) and (11) (with $\mathbf{S}_{\xi}$ from Eq. (14)) has been already proved analytically in Section 2.4. We have further verified that they provide a PSD very close to the kMC results considering a wide variety of Markov chains with various topologies and rates. In this section, we report some examples relevant to bio-chemical sensing based on particles/molecules adsorption-desorption on surfaces.

3.1. pH sensing with Pt surface

As a relevant example, we consider the PSD of the surface charge fluctuation on a Pt surface for different pH of the sample electrolyte. Parameters of the site binding model have been calibrated in [19].

The Markov chain of the chemical reactions is sketched in Fig. 3 and the model parameters are reported in Table 1. The molar concentration

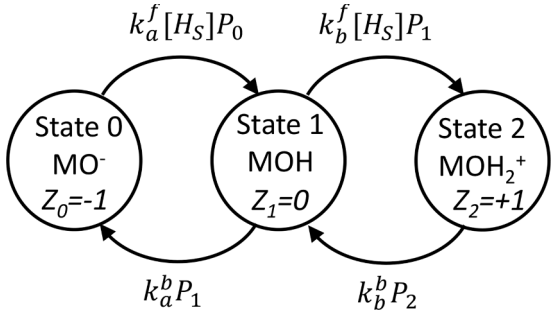

Fig. 3. Markov chain of the site binding model. The protonation of state 0 (i.e. MO^- site) with probability per unit time $k_a^f[H_S]P_0$ moves the site to state 1 (MOH). This can be further protonated with probability per unit time $k_b^f[H_S]P_1$ and moves to state 2 (MOH_2^+). States 1 and 2 are de-protonated with rate $k_a^bP_1$ and $k_b^bP_2$, respectively. k_a^f, k_b^f, k_a^b and k_b^b are the reaction rate coefficients of the different surafce reactions. $[H_S]$ is the concentration of protons in the proximity of the sensing surface.

Table 1
Model parameters for the site-binding model of Fig. 3 taken from Bellando et al. [19]. M stands for mol/L.

Parameters	Value	Meaning
k_a^f	$1.05{\cdot}10^4$ $(\mathrm{Ms})^{-1}$	forward reaction rate coefficient for protonation of state MO^-
k_a^b	0.1053 s^{-1}	backward reaction rate coefficient for protonation of state MO^-
k_b^f	$1.43{\cdot}10^6$ $(\mathrm{Ms})^{-1}$	forward reaction rate coefficient for protonation of state MOH
k_b^b	0.1429 s^{-1}	backward reaction rate coefficient for protonation of state MOH
N_S	$5.5{\cdot}10^{16}$ m^{-2}	sites per unit area
A	1 μm^2	area of the sensing surface

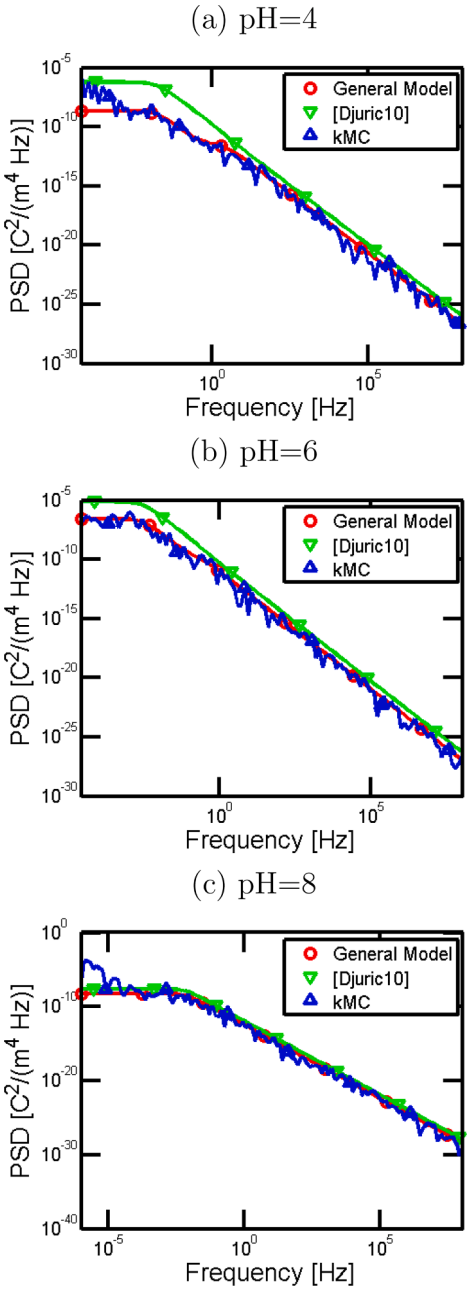

Fig. 4. Simulated PSD of the charge fluctuation per unit area for pH sensing using a Pt surface. The label *general model* refers to Eq. (9) that is completely equivalent to Eq. (11) using Eq. (14). The label *Djuric10* refers to Eq. (11) using Eq. (13) from Djurić et al. [11]. The figure also reports the kMC results.

of protons at the surface is computed as

$$[H_S] = 10^{-pH}\exp\left(-\frac{q\psi_S}{K_B T}\right) \tag{26}$$

where the surface electrostatic potential ψ_S (considering as reference the potential in the bulk of the electrolyte) has been computed by solving the Poisson-Boltzmann equation assuming a background NaCl concentration of 50 mM. The number of sites is just the product between the concentration of sites per area N_S extracted in [19] and the surface area A.

The topology of the Markov chain in Fig. 3 can be interpreted both as a chained process (numbering as state '0' the one on the left, as done in the figure) or as branched one (numbering as '0' the state in the middle). When employing the *general* model (i.e. either Eqs. (9) or (11) with $\mathbf{S}_\xi$ from Eq. (14)), the numbering of the states does not matter. If the Markov chain is intended as branched, one can use $\mathbf{S}_\xi$ from Eq. (12) together with Eq. (11) and get exactly the same results as using the general model (not shown).

Fig. 4 shows that the general model closely follows the kMC results, which confirms the correctness of Eq. (9) (and of Eq. (11) with $\mathbf{S}_\xi$ from Eq. (14)). When one instead uses for Eq. (11) the expression of $\mathbf{S}_\xi$ from Eq. (13), the results deviate from the kMC.

It is worth noting that in this analysis we kept frozen the surface electrostatic potential ψ_S, which means keeping constant the concentration of protons in proximity of the surface (see Eq. (26)). Indeed our aim is to compare the different modeling approaches to compute the surface charge fluctuations for given parameters of the Markov chain. However, the charge fluctuations associated to stochastic binding/unbinding result in potential fluctuations and eventually in fluctuations of the concentration of protons close to the sensing surface. However, factors such as the density of sites per unit area and the background ionic strength of the solution can minimize the extent of these fluctuations. A powerful way to account for potential fluctuation is through an equivalent circuit, as extensively discussed in [10,19].

3.2. Competitive binding of neutral molecules on a surface

We now consider the competitive binding of neutral molecules on a finite set of sites present on a surface. This phenomenon and the associated fluctuation noise have been extensively studied in [12,16].

Assuming that all sites are independent (we will extensively discuss

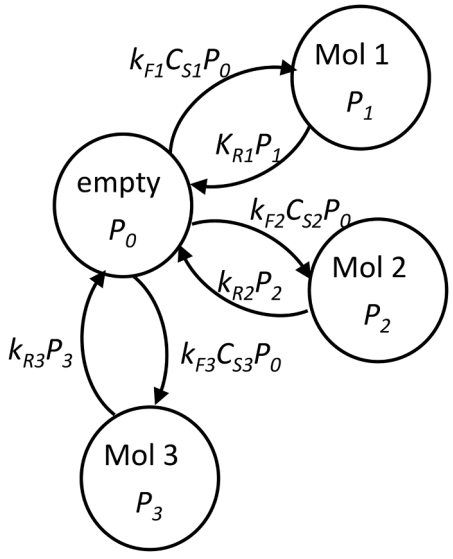

Fig. 5. Graphs describing the time evolution of the Markov chain for the competitive binding of three different types of molecules on a sensing surface. The label "Mol X" stands for "site occupied by the molecule of type X".

this point later), the process can be described by a Markov chain with branched topology, see Fig. 5: the site can be either empty or occupied by one of the molecules (three different types in the figure and in the following results). The adsorption rate is proportional to the concentration (C_{Si}) of molecules of species i in proximity of the surface multiplied by the forward reaction rate k_{Fi}. The desorption rate is indicated as k_{Ri}.

The vector $\mathbf{x}$ contains the mass of the molecules of different species:

$$\mathbf{x} = [0, m_1, m_2, m_3] \tag{27}$$

As long as the surface concentration of the species is constant over time, the occupations of the different sites are uncorrelated and one can use the theory presented in the previous section. However, as discussed in [12,16], the surface concentrations indeed depend on the occupation of the sites. In fact, in steady-state conditions, the flux of particles from the bulk of the electrolyte toward the surface can balance with the adsorption/desorption rate:

$$Ak_{mi}(C_{Oi} - C_{Si})N_A 10^3 = k_{Fi}C_{Si}\left(N_{sites} - \sum_j N_j\right) - k_{Ri}N_i \tag{28}$$

where N_A is Avogadro's number, the C_{Oi} are the concentrations in the bulk of the electrolyte in mol/L and the factor 10^3 converts m^3 in liters. The k_{mi} are kinetic parameters ruling the mass transfer from the bulk of the electrolyte toward the sensing surface. The flux of molecules of species i toward the surface is assumed to be proportional to the difference between C_{Oi} and C_{Si}. N_i is the number of molecules of ith species bound on the surface. On the other hand, the factors k_{Fi} and k_{Ri} control the binding/unbinding of the molecules on the sensing surface. Eq. (28) gives:

$$C_{Si} = \frac{C_{Oi} + k_{Ri}N_i/\left(k_{mi}AN_A 10^3\right)}{1 + k_{Fi}\left(N_{sites} - \sum_j N_j\right)/\left(k_{mi}AN_A 10^3\right)} \tag{29}$$

A proper treatment of the fluctuation should then go beyond the approximation of independent sites embraced by the models analyzed in this work. Even the kMC algorithm described in Section 2.5 is not adequate for that. In the following, we thus assume $k_m \to \infty$ so that $C_{Si} = C_{Oi}$. We will discuss the more general case in Section 4. With this assumption, we can use the kMC and compare it with the general model (i.e., either Eqs. (9) or (11) with $\mathbf{S}_\xi$ from Eq. (14)). It can be demonstrated analytically that the general model fully matches the model in [12] when $k_m \to \infty$, so that only the general model is plotted in the comparison between model and kMC shown in Fig. 6.

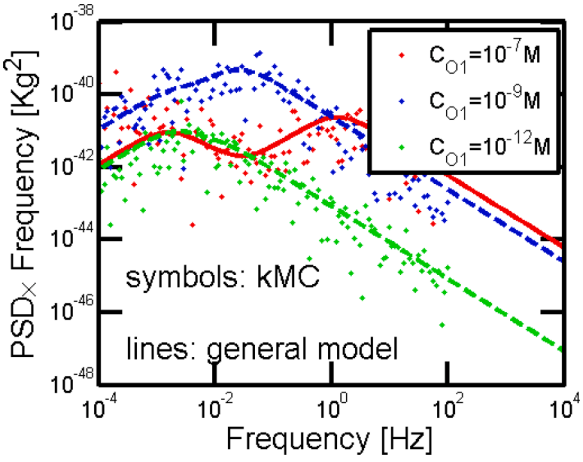

Fig. 6. Simulated PSD (multiplied by the frequency) of the mass fluctuation related to competitive binding of molecules on a surface. The *general model* (i.e. Eq. (9) that is completely equivalent to Eq. (11) using Eq. (14)) is compared with the kMC results. Parameters are reported in Table 2, except that k_{mi} are set to infinity.

Table 2
Model parameters for the competitive binding of molecules on a surface.

Parameters	Molecule 1	Molecule 2	Molecule 3	Units
C_{Oi}	varied	5×10^{-8}	10^{-7}	M
k_{Fi}	8×10^7	4×10^4	3.2×10^4	$M^{-1}s^{-1}$
k_{Ri}	0.08	0.01	0.01	s^{-1}
k_{mi}	5×10^{-6}	10^{-6}	10^{-6}	m/s
N_{sites}/A		3×10^{15}		m^{-2}
A		10^{-9}		m^2

The simulation parameters are reported in Table 2. The ratios k_{Fi}/k_{Ri}, the bulk concentrations, and the number of sites are taken from [12]. We set the rates k_{Ri} to reproduce the PSD reported in [12].

When implementing the general model, the state *0* (empty site) of Fig. 5 has been removed, and the equilibrium occupation probabilities needed in Eq. (10) are computed as [12]:

$$P_i^0 = \frac{\frac{k_{Fi}}{k_{Ri}}C_{Oi}}{1 + \sum_{j=1}^{3}\frac{k_{Fj}}{k_{Rj}}C_{Oj}}. \tag{30}$$

Fig. 6 shows the perfect agreement between the kMC results and the general model discussed in this paper. As stated above, the general model is fully consistent (it can be proven analytically with tedious calculations not reported here) with the model for competitive binding presented in [12]. The latter can be applied also to the case when the k_{mi} are finite, as we will see in Section 4.

3.3. Multi-layer adsorption of neutral molecules

In this section, we consider the adsorption of a single species (electrically neutral) on a finite number of independent surface sites. Molecules/particles can pile up and create more than one layer. This situation has been analyzed in [11] and can be summarized with the Markov chain in Fig. 7: each site can bind an increasing number of particles. In principle, the chain should extend to infinity, but we limited it to a maximum number of $n = 10$ particles per site and verified that this number is large enough to make the results independent of this choice.

The detaching rate from state k goes as

$$\tau_k = \tau_0 \exp\frac{E_{dk}}{RT} \tag{31}$$

where $\tau_0 = 0.1$ ps and the detaching energies are $E_{d1-6} = 15.5/12.5/10.5/10/9.5/9$ kcal/mol, $E_{dk} = 8$ kcal/mol for $k > 6$ [11]. The adsorption rate is given by $a_k \cdot p$, where p is the pressure in the chamber and

$$a_k = \frac{\alpha_{Sk}}{(N_{sites}/A)\sqrt{2\pi M_a k_B T}} \tag{32}$$

where $M_a = 28$ Da [20] is the mass of the adsorbed particle and we set $\alpha_{Sk} = 1$ for all k (i.e., we assume that all molecules hitting the sensing surface are adsorbed). The density of sites is $N_{sites}/A = 10^{18}$ m^{-2} [11]. The temperature is $T = 300$ K. Eq. (32) can be easily derived bearing in mind that, since α_{Sk} is the probability for a molecule impinging the surface to be adsorbed, $a_k p/\alpha_{Sk}$ is the number of molecules per unit time hitting the area belonging to one site (assumed to be the total area of the sensing surface divided by the number of sites). According to Boltzmann statistics, the molecules impinging the surface have an average velocity normal to the surface equal to $\overline{|v_\perp|} = \sqrt{2k_B T/(\pi M_a)}$. The flux impinging the surface is $\overline{|v_\perp|}N_A c/2$, where c is the molar concentration of the molecules in the chamber and the factor $1/2$ stands from the fact that only half of them are oriented toward the surface. The law of ideal gases states that the pressure in the chamber is $p = cN_A k_B T$. Putting all together:

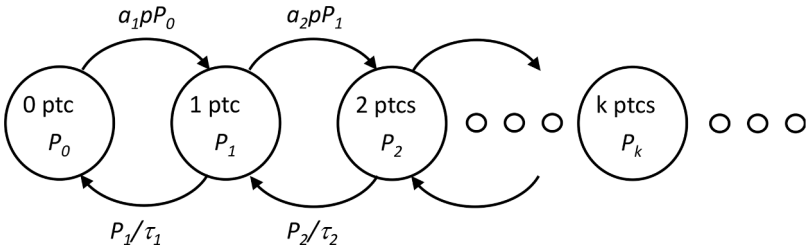

Fig. 7. Graphs describing the time evolution of the Markov chain for the multi-layer adsorption of particles on a surface.

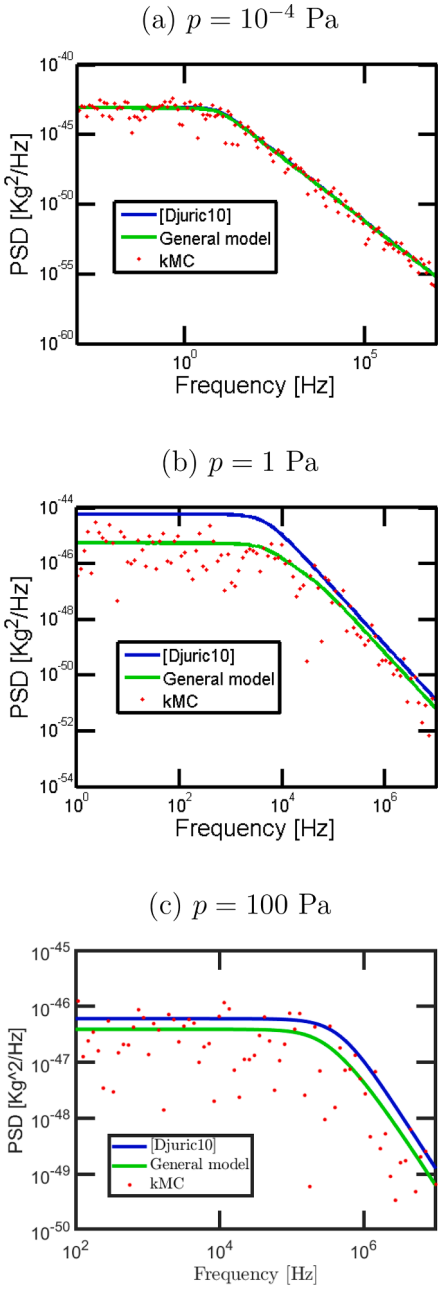

Fig. 8. Simulated PSD of the mass fluctuation in the case of multi-layer adsorption on a sensing surface. The label *general model* refers to Eq. (9) that is completely equivalent to Eq. (11) using Eq. (14). The label *Djuric10* refers to Eq. (11) using Eq. (13) from Djurić et al. [11]. The figure also reports the kMC results.

$$\frac{a_k p}{\alpha_{Sk}} = \overline{|v_\perp|} N_A \frac{c}{2} \frac{A}{N_{sites}} = \sqrt{\frac{2k_B T}{\pi M_a}} \frac{1}{2} \frac{p}{k_B T} \frac{A}{N_{sites}} \tag{33}$$

which gives Eq. (32).

The vector $\mathbf{x}$ associated to the Markov chain in Fig. 7 contains the mass adsorbed in the single site for each state:

$$\mathbf{x} = [0, M_a, \cdots, kM_a, \cdots, nM_a] \tag{34}$$

When applying the general model, we construct the matrices T and R to eliminate state 0.

It is easy to show that the occupation probabilities at equilibrium are given as

$$P_k^0 = \frac{\alpha_1 \cdots \alpha_k}{1 + \alpha_1 + \cdots + \alpha_1 \cdots \alpha_k + \cdots + \alpha_1 \cdots \alpha_n} \tag{35}$$

where $\alpha_k = a_k p \tau_k$. One can easily see that if all α_k are larger than 1, the occupation probabilities increase with k (i.e., more probable to have many layers per site), meaning that the probability of state n is the largest and tends to be close to 1. If one increases n, this 1 just moves to the last state, i.e., the system is unstable and the number of layers grows indefinitely over time. With the parameters employed here, this happens when p is larger than approximately 500 Pa. For this reason, we have limited our analysis to $p \leq 100$ Pa.

Results are reported in Fig. 8. As expected, for low pressure (top graph) the general model discussed in this paper (that is Eq. (9) or, equivalently, Eq. (11) using Eq. (14)) and the model in [11] (i.e. Eq. (11) using Eq. (13) and with all elements of $\mathbf{x}$ equal to M_a as from Eq. (5) in [11]) are very close, since all sites capture at most one single molecule and the noise follows the Langmuir model as already shown in [11]. When the pressure increases (middle and bottom graphs in Fig. 8) the two models start to deviate, and only the general model matches the kMC results (although the kMC becomes very noisy at high pressures, requiring extremely long simulation times). As discussed previously, the main reason for this difference is that Eq. (13) used in [11] should be replaced by Eq. (15). Furthermore, the elements of $\mathbf{x}$ should not be all equal to M_a as in [11], but, instead, follow Eq. (34). When these two aspects are modified into the model of [11], it becomes coincident with the general model, as can be shown analytically and demonstrated numerically (not shown in the plots since these curves are perfectly overlapped).

4. Correlation between sites in the case of competitive binding

The main limitation of the approach analyzed here (summarized by either Eq. (9) or by Eq. (11) with $\mathbf{S}_\xi$ from Eq. (14)) is that it assumes that all sites are independent. This allows us to compute the PSD of the fluctuation of a single site using the matrix $\mathbf{\Gamma}$ obtained via Eq. (10) and then just multiply by the number of sites. If the occupation of the sites is correlated, this approach cannot be used. A relevant case study is the competitive binding of molecules, analyzed in Section 3.2: the molecule's concentration at the surface is given by Eq. (29) and depends on the actual number of molecules bound on the surface. It is easy to show that the equilibrium concentration on the surface (that is obtained from

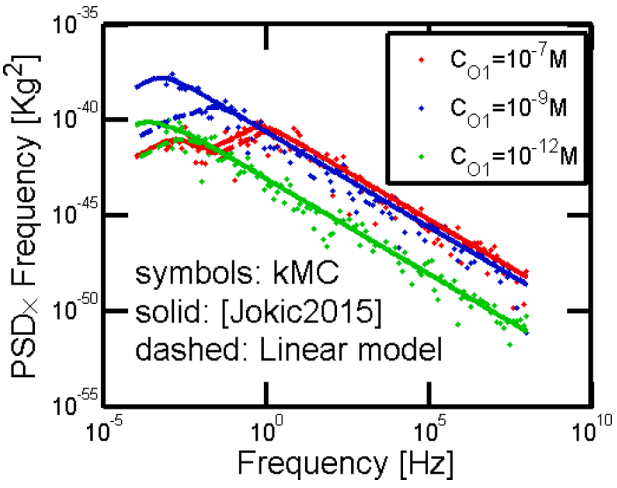

Fig. 9. Product between fluctuation PSD and frequency for the case of competitive binding of 3 different molecules on a surface. Compared to the analysis presented in Section 3.2, here the effect of the number of bound molecules on the surface concentrations is taken into account. Model parameters are from Table 2. The kMC results are compared with the model proposed in [12] and with the model presented in this work (Eq. (9) or, equivalently, Eq. (11) coupled with Eq. (14) of Eq. (12)), indicated as *linear model* since it does not account for the effect of the number of bound molecules on the transition rate.

Eq. (29) writing $N_i = N_{sites}P_i^0$) is equal to the bulk concentration C_{Oi}. However when N_i fluctuates, C_{Si} fluctuates too, so that the transition rates for a given site would depend on the occupation of the other site. The analytical solution for this situation has been derived in [12]. The model employs Eq. (11), the expressions for $\mathbf{\Omega}$ and $\boldsymbol{S}_{\xi}$ are reported in the reference. To validate that model and compare it with the case of independent sites, we have developed a kMC algorithm specific to this problem. We know from [12] that the time evolution of the number of molecules of species i on the surface follows:

$$\frac{dN_i}{dt} = k_{Fi}\frac{C_{Oi} + k_{Ri}N_i/\left(k_m A N_A 10^3\right)}{1 + k_{Fi}\left(N_{sites} - \sum_j N_j\right)/\left(k_m A N_A 10^3\right)}\left(N_{sites} - \sum_j N_j\right) - k_{Ri}N_i, \tag{36}$$

as can it be easily derived from the Markov chain in Fig. 5 expressing the C_{Si} from Eq. (29). In the kMC, the first term at the r.h.s. of Eq. (36) is the probability per unit time to increase N_i by 1, while the second term is the probability per unit time to decrease N_i by 1. These probabilities need to be recomputed after each event. The adsorbed mass is then computed as $\sum_i N_i m_i$ and the PSD of the fluctuations is computed as in Section 2.5.

Fig. 9 shows that the model proposed in [12] (solid lines) nicely matches the kMC results (symbols). The figure also reports the results obtained with the models discussed in this paper (that are all equivalent in the case of branched reactions). These models assume independent sites and deviate from the kMC results at low frequencies.

Although the correlation between sites occupation due to mass transfer from the bulk toward the surface has an effect on fluctuation noise, it has no effect on the sensor response. The response is indeed given by the steady-state occupation of the sites. This can be found by setting to zero the time derivatives in Eq. (36). With simple calculations one can find that the fraction of sites bound with molecules of type i is given by:

$$\frac{N_i^0}{N_m} = \frac{\frac{k_{Fi}}{k_{Ri}}C_{Oi}}{1 + \sum_{j=1}^{3}\frac{k_{Fj}}{k_{Rj}}C_{Oj}}. \tag{37}$$

We see that the k_{mi} terms disappear so the results are the same as for independent sites (Eq. (30)). The sensor response (i.e. the surface mass

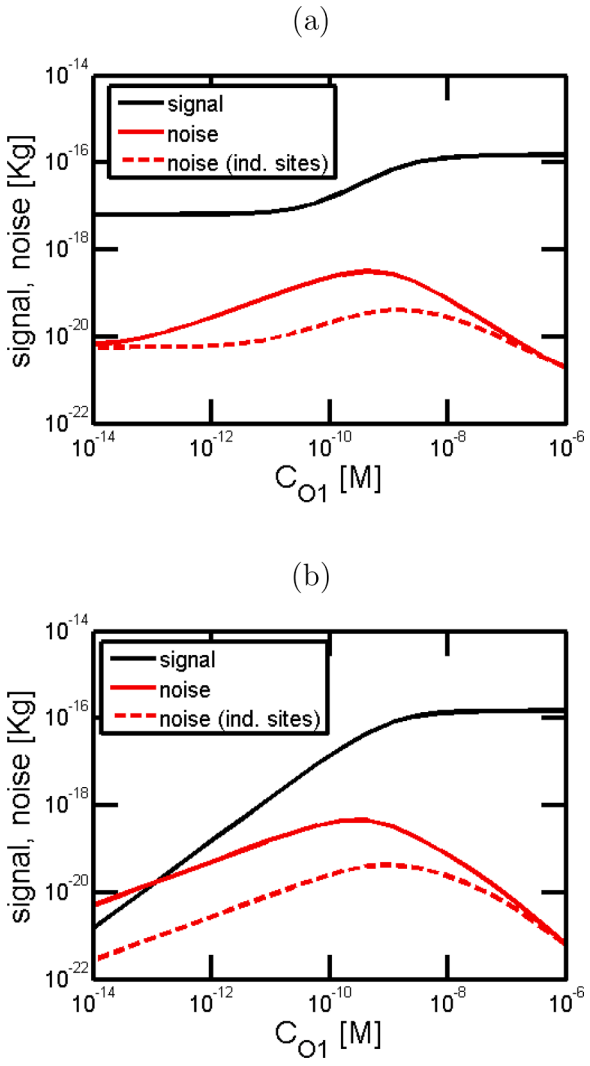

Fig. 10. Signal (black curve) and noise (red curves) for the case of competitive binding of molecules on a sensing surface. The noise trace is the integral of the PSD in the band from 0 to 1Hz. The red solid curve has been obtained from the model proposed in [12] (that includes correlation between sites), while the red dashed curve with the model presented in this work, that assumes independent sites. Plot (a) uses the default parameters from Table 2, while in plot (b) we set C_{O2} and C_{O3} to zero. (For interpretation of the references to colour in this figure legend, the reader is referred to the web version of this article.)

given as $m_1N_1 + m_2N_2 + m_3N_3$ to the bulk concentration of molecules of type 1 is reported in Fig. 10 either considering the simulation parameters of Table 2 (plot a) or setting to zero the concentration of interfering molecules of type 2 and 3. In both cases, we see a plateau at high concentrations due to saturation of the binding sites. The presence of interfering molecules (plot a) induces a plateau also at low concentration (i.e., the sensor responds to the interfering molecules), whereas when only the target molecules are present, the response is proportional to the bulk concentration of the target molecules.

The r.m.s. value of the noise (i.e., the square root of the PSD integrated over a bandwidth from 0 to 1Hz) has been plotted by comparison using either the model for correlated sites (red solid line) or the model for independent sites (red dashed line). We see that, consistently with the previous analysis, correlation between sites has an effect of noise. While in the presence of interfering molecules (plot a) the sensor response at low concentration is limited by surface selectivity to the target molecules, when only target molecules are present with low concentration, noise becomes the limiting factor (plot b). In this

situation, the estimation of the lower-limit-of-detection significantly changes considering independent sites.

5. Conclusions

We have shown that the model for fluctuation noise due to adsorption/desorption of particles on a surface proposed in [10] using the simplified forward Kolmogorov equation is fully consistent with the models based on Langevin sources proposed in different papers [11,12], although the model in [11] should be modified by considering the non-diagonal terms in the $\mathbf{S}_{\xi}$ matrix. We have also shown that the models in [11,12] can be generalized following the approaches for fluctuation noise discussed in [17], while the original papers were dealing with particular cases. This generalized formulation is completely equivalent to the one in [10].

The main limitation of these general approaches, however, is that they assume that all sites are independent. This limitation was overcome in [12] for the particular case of competitive binding. Developing a model able to account for correlation between sites in general cases would be an interesting future perspective, but is well beyond the scope of this work.

Declaration of Competing Interest

The authors declare that they have no known competing financial interests or personal relationships that could have appeared to influence the work reported in this paper.

Data availability

Data will be made available on request.

References

[1] A.J. Bard, L.R. Faulkner, H.S. White, Electrochemical Methods: Fundamentals and Applications, second ed., John Wiley & Sons Inc, 2001.
[2] P. Bergveld, Thirty years of ISFETOLOGY: what happened in the past 30 years and what may happen in the next 30 years, Sens. Actuators B Chem. 88 (1) (2003) 1–20.
[3] D.E. Yates, S. Levine, T.W. Healy, Site-binding model of the electrical double layer at the oxide/water interface, J. Chem. Soc. Faraday Trans. 1 Phys. Chem. Condensed Phase 70 (1974) 1807–1818.
[4] R.E.G.V. Hal, J.C.T. Eijkel, P. Bergveld, A general model to describe the electrostatic potential at electrolyte oxide interfaces, Adv. Colloid Interface Sci. 69 (1–3) (1996) 31–62.
[5] G. Zheng, X.P.A. Gao, C.M. Lieber, Frequency domain detection of biomolecules using silicon nanowire biosensors, Nano Lett. 10 (8) (2010) 3179–3183.
[6] D. Zhang, P. Solomon, S.L. Zhang, Z. Zhang, An impedance model for the low-frequency noise originating from the dynamic hydrogen ion reactivity at the solid/liquid interface,, Sens. Actuators B Chem. 254 (2018) 363–369.
[7] Q. Guo, T. Kong, R. Su, Q. Zhang, G. Cheng, Noise spectroscopy as an equilibrium analysis tool for highly sensitive electrical biosensing, Appl. Phys. Lett. 101 (9) (2012), 093704.
[8] A. Hassibi, S. Zahedi, R. Navid, R.W. Dutton, T.H. Lee, Biological shot-noise and quantum-limited signal-to-noise ratio in affinity-based biosensors,, J. Appl. Phys. 97 (8) (2005) 084701.
[9] T. Contaret, J.-L. Seguin, P. Menini, K. Aguir, Physical-based characterization of noise responses in metal-oxide gas sensors, IEEE Sens. J. 13 (3) (2013) 980–986.
[10] L.J. Mele, P. Palestri, L. Selmi, General model and equivalent circuit for the chemical noise spectrum associated to surface charge fluctuation in potentiometric sensors, IEEE Sens. J. 21 (5) (2021) 2021–6258.
[11] Z.G. Djurić, I.M. Jokić, M.M. . Djukić, M.P. Frantlović, Fluctuations of the adsorbed mass and the resonant frequency of vibrating MEMS/NEMS structures due to multilayer adsorption, Microelectron. Eng. 87 (2010) 1181–1184.
[12] I. Jokić, M. Frantlović, Z. Djurić, K. Radulović, Z. Jokić, Adsorption-desorption noise in microfluidic biosensors operating in multianalyte environments, Microelectron. Eng. 144 (2015) 32–36.
[13] L.J. Mele, P. Palestri, L. Selmi, General approach to model the surface charge induced by multiple surface chemical reactions in potentiometric FET sensors, IEEE Trans. Electron. Devices 67 (3) (2020) 1149–1156.
[14] K.T. Radulović, I.M. Jokić, M.P. Frantlović, Z.G. Djurić, Adsorption-desorption noise in nanowire FET biosensors. Proc. 28th International Conference on Microelectronics (Miel 2012), Nis, Serbia, 13–16 May, 2012, pp. 203–206.
[15] M. Frantlović, I. Jokić, Z. Djurić, K. Radulović, Analysis of the competitive adsorption and mass transfer influence on equilibrium mass fluctuations in affinity-based biosensors, Sens. Actuators B 189 (2013) 71–79.
[16] I. Jokić, Z. Djurić, M. Frantlović, K. Radulović, P. Krstajić, Z. Jokić, Fluctuations of the number of adsorbed molecules in biosensors due to stochastic adsorption-desorption processes coupled with mass transfer, Sens. Actuators B 166–167 (2012) 535–543.
[17] C.M.V. Vliet, Macroscopic and microscopic methods for noise in devices, IEEE Trans. Electron. Devices 41 (11) (1994) 1902–1915.
[18] A.D. Trigilio, Y.W. Marien, P.H.M.V. Steenberge, D.R. D'hooge, Gillespie-driven kinetic Monte Carlo algorithms to model events for bulk or solution (bio) chemical systems containing elemental and distributed species, Ind. Eng. Chem. Res. 59 (41) (2020) 18357–18386.
[19] F. Bellando, L.J. Mele, P. Palestri, J. Zhang, A.M. Ionescu, L. Selmi, Sensitivity, noise and resolution in a BEOL-modified foundry-made ISFET with miniaturized reference electrode for wearable point-of-care applications, MDPI Sensors 21 (2021) 1779.
[20] Z. Djurić, I. Jokić, M. Frantlović, O. Jakšić, Fluctuations of the number of particles and mass adsorbed on the sensor surface surrounded by a mixture of an arbitrary number of gases, Sens. Actuators B Chem. 127 (2) (2007) 625–631.